ESR studies of the spin dynamics in quasi-one-dimensional iodo-bridged diplatinum complex $Pt_2(n\text{-pentylCS}_2)_4I$

Hisaaki Tanaka,[1] Shin-ichi Kuroda,[1] Takami Yamashita,[2] Minoru Mitsumi,[2] and Koshiro Toriumi[2]
[1]*Department of Applied Physics, Nagoya University, Furo-cho, Chikusa-ku, Nagoya 464-8603, Japan*
[2]*Graduate School of Material Science, University of Hyogo, 3-2-1 Kouto, Kamigori-cho, Hyogo 678-1297, Japan*
(Received 2 November 2005; revised manuscript received 10 March 2006; published 7 June 2006)

ESR measurements have been performed on a quasi-one-dimensional (Q1D) halogen-bridged binuclear metal-complex $Pt_2(n\text{-pentylCS}_2)_4I$ which exhibits successive electronic phase transitions. Anisotropy of the ESR linewidth shows a drastic change around 215 K where the phase transition takes place between a nonmagnetic alternate-charge-polarization (ACP) state for low temperatures and a paramagnetic averaged-valence (AV) state with a relatively good electrical conductivity for higher temperatures. In the AV state, a clear minimum of the linewidth is observed around 50° from the chain direction due to the contribution of the secular 1D dipolar term varying as $3\cos^2\theta-1$, where θ denotes the angle between the external magnetic field and the chain axis. In addition to the dipolar contribution, the linewidth also exhibits temperature-dependent spin-phonon contribution. These features of linewidths are consistent with those reported previously for Q1D conductors such as charge transfer salts and Pt-complexes, providing microscopic evidence for the occurrence of a Q1D conduction-electron system in the present bimetal complex. In the ACP state, the spin concentration drastically decreases due to the nonmagnetic nature of the background electronic state. The linewidth shows a uniaxial anisotropy with respect to the chain axis, which can be reasonably ascribed to the anisotropy of unresolved hyperfine structures due to Pt and iodine nuclear spins. The spin susceptibility shows a clear enhancement from Curie-type behavior, accompanied with a change of the line shape from a nearly Gaussian at 4 K to Lorentzian with motional narrowing as the temperature is raised. The results further support our previous conjecture that the observed spins are thermally excited solitons.

DOI: 10.1103/PhysRevB.73.245102 PACS number(s): 71.30.+h, 76.30.−v, 76.30.Pk, 76.30.He

I. INTRODUCTION

There has been increasing attention focused on quasi-one-dimensional (Q1D) electron systems owing to their interesting electrical, optical, and magnetic properties.[1–3] Systems studied so far include both organic and inorganic materials. The former case includes organic conductors or semiconductors such as charge transfer salts and conjugated polymers. The latter case covers inorganic materials like inorganic polymers, transition-metal chalcogenides, and transition metal complexes such as $K_2Pt(CN)_4Br_{0.3}\cdot 3H_2O$ (KCP). Various electronic states have been clarified in those materials; metallic states, charge-density-wave (CDW) states, Mott-Hubbard states, spin-Peierls states, and so on.[2,3] Nonlinear excitations, such as solitons, polarons, and bipolarons, in these Q1D systems have also been extensively studied both theoretically and experimentally, in particular, in conjugated polymers.[4,5]

For more than two decades, halogen(X)-bridged metal(M) complexes, so-called MX-[2,3,6–9] or MMX-chain complexes,[10–18] are one of the most well-investigated Q1D materials owing to their wide variety of physical properties. In MX-chain complexes, the electronic ground state is sensitive to the electron-phonon interaction (S) and on-site Coulomb interaction (U). Depending on the relative magnitude of U and S, the electronic ground state is classified into either the mixed-valence CDW state $[\cdots M^{2+}\cdots X^{-}-M^{4+}-X^{-}\cdots]$ (M=Pt,Pd) for $S>U$ or monovalence Mott-Hubbard state $[-M^{3+}-X^{-}-]$ (M=Ni) for $S<U$.[6–8] Here, dotted ($\cdots$) and solid (–) lines in the CDW state represent the longer and shorter metal–halogen bonds, respectively. The optically induced soliton and polaron have been so far investigated in the CDW states.[9,19] On the other hand, gigantic third-order optical nonlinearity,[20] ultrafast insulator-metal switching,[21] or the formation of spin-Peierls ground state[22] have been reported for the Mott-Hubbard systems such as $Ni(chxn)_2Br_3$ (chxn=1R-, 2R-cychlohexanediamine). A series of mixed-metal complexes $Ni_{1-x}Pd_x(chxn)_2Br_3$ have also been successfully synthesized and the conversion of the CDW state (Pd^{2+}-Pd^{4+}) into the Mott-Hubbard state (Pd^{3+}) due to the competition of U and S has been demonstrated.[23–28] In particular, ESR measurements have played an essential role to clarify the conversion of CDW to Mott-Hubbard states as the direct method to detect the magnetic Pd^{3+} ions occurring in the Mott-Hubbard state.[24,26] The concentration dependence of the conversion has been well-reproduced by theoretical calculations[28,29] or more recently, by the direct observation of the valence ordering patterns by scanning tunnel microscope measurements.[27]

In recent years, more sophisticated MMX-chain complexes have been attracting much interest.[10–17,30–45] In these complexes, direct metal-metal bonding creates various kinds of valence ordering patterns, typically represented as:

(a) averaged-valence (AV) state
$[-M^{2.5+}-M^{2.5+}-X^{-}-M^{2.5+}-M^{2.5+}-X^{-}-]$,
(b) CDW state
$[\cdots M^{2+}-M^{2+}\cdots X^{-}-M^{3+}-M^{3+}-X^{-}\cdots]$,
(c) charge-polarization (CP) state
$[\cdots M^{2+}-M^{3+}-X^{-}\cdots M^{2+}-M^{3+}-X^{-}\cdots]$, and
(d) alternate-charge-polarization (ACP) state
$[\cdots M^{2+}-M^{3+}-X^{-}-M^{3+}-M^{2+}\cdots X^{-}\cdots]$.

Here, AV and CP states have finite spin densities on the chain with unpaired electrons on the M^{3+} ions whereas CDW and

ACP states are nonmagnetic due to the formation of intra- and inter-dimer spin-singlet states, respectively. The AV state is expected to become metallic when the Coulomb repulsion is weak. In fact, Kitagawa *et al.* reported for the first time among the *MX*-or *MMX*-chains that the iodo-bridged diplatinum complex, $Pt_2(RCS_2)_4I$ ($R=CH_3$), shows metallic transport property above 300 K.[16] Moreover, this complex undergoes metal-insulator transition below room temperature due to the formation of a possible CP state, and further transition occurs around 80 K by forming the ACP state.[16] Furthermore, Mitsumi and co-workers have successfully synthesized a series of *MMX*-chain complexes of $Pt_2(RCS_2)_2I$ (R=ethyl,[32] *n*-propyl,[33] *n*-butyl,[34] and *n*-pentyl,[35]), with the strategy of tuning the interchain interaction by employing various alkyl chain (R) lengths of the ligand molecules. Detailed x-ray analyses of single crystals have revealed that several structural transitions occur in these systems involving the rearrangement of the valence ordering patterns depending on the length of R. The ESR method has also been successfully applied in studying the nature the electronic states and nonlinear excitations in the case of $R=n$-butyl and *n*-pentyl analogs.[36]

Before describing the relevant ESR results, a summary of the electronic phases of these complexes is given as follows. In the complex with $R=n$-butyl, three phases have been reported as follows: an AV state with metallic transport properties above 324 K, an AV state with threefold Pt-Pt-I unit-repetition due to the structural inhomogeneity of the ligand molecules in $324\ K > T > 210$ K, and an ACP state below 210 K.[34,39] Similarly, the electronic phase of the complex with $R=n$-pentyl is divided into three phases by the first- and second-order phase transitions at approximately 270 and 324 K, respectively.[35,41] The room temperature (RT) phase of this complex is an AV state with a threefold Pt-Pt-I unit repetition, although the definitive determinations of the valence-ordering states or precise crystal structures for other phases have not been completed yet. In addition, metallic electronic conductivity is reported above 240 K, implying that the high-temperature (HT) phase is also an AV state as in the case of $R=n$-butyl.[34,35] The crystal structure at 253 K (RT phase) is shown in Fig. 1.[35,41] The crystal belongs to the tetragonal space group with its *c*-axis parallel to the chain axis.

As for the ESR results, both complexes showed significant changes in ESR spectra at approximately 210 K, caused by the first-order phase transition between the AV state of the RT phase and the ACP state of the low-temperature (LT) phase.[36] In addition, in the LT phase of the complex with $R=n$-pentyl, we have suggested the thermal excitation of the soliton kink of Pt^{3+} from the spin concentration enhancement and the motional narrowing of ESR spectra above about 20 K. This is the first experimental observation of the soliton in *MMX*-chains, whose existence has already been predicted theoretically.[46–48] No report, however, has been made concerning the anisotropy of ESR spectra using single crystals, which can probe spin dynamics in relevant phases. In this paper, we report a detailed single crystalline ESR study of the above complex with $R=n$-pentyl to get a further insight into the soliton excitation and the nature of the insulating ACP and the conducting AV states. As for the temperature range of the measurement in the present study, we extended the upper limit from room temperature (about 300 K) of our previous study up to 364 K. This enabled us to cover the above-mentioned upper phase transition temperature of 324 K between the RT phase and HT phase in the AV-state region. We present the detailed angular dependence of *g*-value and linewidth for those three phases. The obtained *g*-tensor components provide clear evidence that the observed spins are associated with the Pt^{3+} state, as is consistent with our previous report.

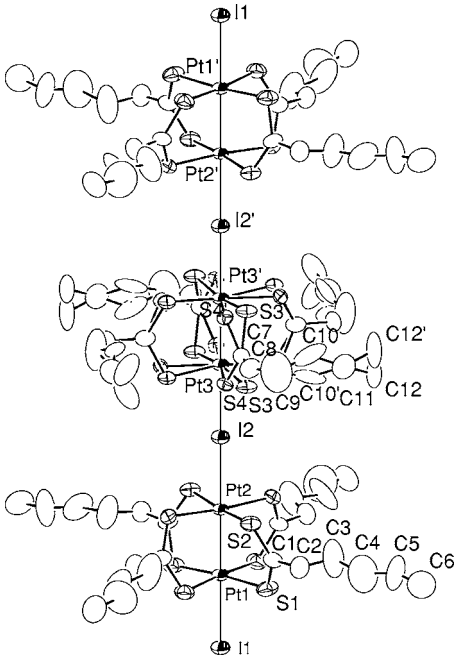

FIG. 1. Crystal structure of $Pt_2(n\text{-pentyl}CS_2)_4I$ obtained at 253 K (RT phase). The *MMX*-chain axis parallel to the *c*-axis is indicated by the straight line.

On the other hand, the angular dependence of the linewidth provides detailed information concerning the spin dynamics in the relevant electronic phases. Generally, the motionally or exchange-narrowed ESR linewidth in Q1D systems is approximately expressed as ω_p^2/ω_e for the extreme narrowing condition of $\omega_e \gg \omega_p$.[49] Here ω_p stands for the static linewidth without the presence of spin motion, while ω_e represents the frequency of the spin flip due to either the spin-motion or spin-exchange. This expression plays a significant role in identifying the occurrence of the narrowing process through the angular dependence of the static linewidth ω_p of which behavior should be dependent on the origin of the static linewidth, such as hyperfine or fine structures in noninteracting spins or spin-spin dipolar coupling in the case of concentrated spins.[50,51]

In the following, we present the angular dependence of the temperature-dependent motionally narrowed ESR linewidth, which has been previously ascribed to the thermally excited solitons in the ACP state.[36] We show that the observed anisotropic behavior in fact approaches to the above expression of ω_p^2/ω_e, where the angular dependence of ω_p is reasonably ascribed to the hyperfine coupling due to Pt or I nuclear spins with uniaxial anisotropies. On the other hand,

the linewidth anisotropy drastically changes at the phase transition temperature from the ACP to AV states occurring around 215 K. It no more shows a uniaxial anisotropy but shows a distinct anisotropy proportional to the square power law of the secular term of the spin-spin dipolar coupling which is closely represented as $3\cos^2\theta-1$. Here θ denotes the angle between the external magnetic field and the one-dimensional *MMX*-chain axis. This contribution becomes zero at the so-called magic angle of about 50°. The linewidth in the AV states above 215 K, however, does not vanish at this angle due to the other significant contribution which shows a practically negligible angular dependence compared with the dipolar contribution. This latter contribution may be reasonably ascribed to the spin-phonon contribution, similar to those reported in the case of Q1D conductors such as charge-transfer salts[52,53] and a metal complex, KCP.[54]

The origin of the above two contributions for the ESR linewidth in the Q1D conducting phase has been discussed as follows. In the Q1D conductors, the spin-phonon contribution from an Elliot mechanism[55] becomes much smaller compared with the case of three-dimensional (3D) metals because of the suppression of either the forward or backward scattering rate due to a flat Q1D Fermi surface. This results in less contribution of the spin-phonon mechanism and the enhanced contribution of spin-spin dipolar mechanism which is usually masked in 3D metals.[52] While the former contribution is weakly angular dependent, the latter, the dipolar contribution, exhibits a unique angular variation, represented by the secular dipolar term as mentioned above. The dominance of the secular dipolar term comes from the long-time tail of the spin correlation function in Q1D spin systems, which washes out the nonsecular contributions due to their oscillations during the lasting tail of the spin correlation function.[49,56,57] The power-law dependence on the secular term changes from $(3\cos^2\theta-1)^{4/3}$ in a pure 1D system to $(3\cos^2\theta-1)^2$ in the Q1D system due to the cut off of the above lasting tail by interchain hopping, resulting in a Lorentzian line shape compared with a non-Lorentzian line shape in the pure 1D system.

Thus the presently obtained angular-dependent ESR linewidth provides microscopic evidence for the occurrence of thermally excited solitons in the ACP state and Q1D conduction-electron systems in the AV states.

II. EXPERIMENT

Samples of $Pt_2(n\text{-pentylCS}_2)_4I$ were prepared by slow cooling of toluene-*n*-hexane solution of equimolar amount of $[Pt_2(n\text{-pentylCS}_2)_4]$ and $[Pt_2(n\text{-pentylCS}_2)_4I_2]$.[34]

ESR measurements were performed by using a Bruker EMX spectrometer at the *X*-band equipped with a gas-flow type cryostat, Oxford ESR-900, for temperatures between room temperature and 4 K. For temperatures above RT up to 364 K, an air-flow-type Bruker ER4111VT unit was used for temperature control. The spin susceptibility was obtained by integrating the first derivative ESR signal twice. The absolute magnitude of the spin susceptibility and *g*-value were calibrated using $CuSO_4\cdot 5H_2O$ and diphenylpicrylhydrazyl (DPPH) as a standard, respectively. Since the ESR spectrum in the AV state has large linewidths of several hundred gauss, more than 200 single crystalline samples were aligned along their *c*-axis on PET (polyethylene-terephthalate) substrates in order to obtain a sufficient signal-to-noise ratio. The use of aligned single crystals does not affect the accurate observation of the anisotropy of ESR signals in the plane containing the chain axis. This is because the observed *g*-values and spectra show uniaxial anisotropy around the chain axis, or negligible orthorhombicity, in other words, as has been reported in the previous study.[36] The spin susceptibility has also been measured using polycrystalline samples at room temperature.[36]

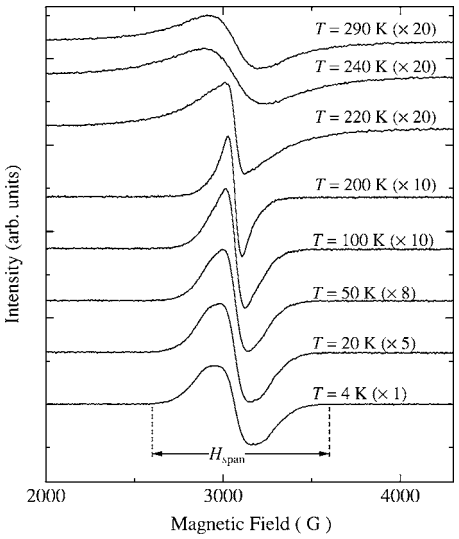

FIG. 2. Temperature dependence of the first derivative ESR spectra of $Pt_2(n\text{-pentylCS}_2)_4I$ with the external magnetic field perpendicular to the *c*-axis together with the definition of spectral span, H_{span} at 4 K (see text of Sec. IV for more details).

III. EXPERIMENTAL RESULTS

Figure 2 shows the temperature dependence of the ESR spectra between RT and 4 K with the external magnetic field *H* perpendicular to the chain axis (*c*-axis). These spectra were recorded in the heating process after initially cooling the sample down to 4 K. A nearly Gaussian-shaped spectrum at 4 K gradually changes to a Lorentzian at 200 K, associated with spectral narrowing, as the temperature is increased in the ACP state below 215 K. This feature is also observed in our previous measurements[36] and is attributed to the motional narrowing phenomena of the spin soliton. The line shape at 200 K is well fit by a Lorentzian. On the other hand, the ESR line shape at 4 K is not a simple Gaussian, but associated with rather flat peaks as in Fig. 2. The flat peaks, however, are not likely to originate from overlapping two kinds of signals with different linewidths, for example, the sharp signal of mobile species and the broad one of static species. In such case, saturation study often discriminates such mobile-spin signals which tend to be more difficult to saturate. In fact, the saturation study of spectral line shape using microwave power up to 200 mW gave no evidence of broad and sharp signals with different saturation behaviors.

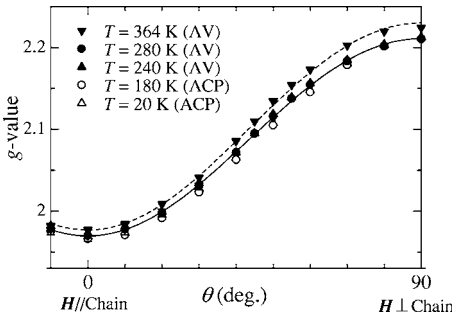

FIG. 3. Angular dependence of the g-value at various temperatures. Solid and dashed lines represent the fitting curves using Eq. (1) for 280 and 364 K, respectively.

Since there are no thermal excitations of spins up to 20 K from susceptibility measurements (Fig. 4), the spectrum at 4 and 20 K may be reasonably ascribed to single spin species, presumably trapped solitons, although there is slight line narrowing at the latter temperature. More detailed discussion will be given later. As for the spectra at higher temperatures at 50 and 100 K, where the thermal excitation of spins becomes more significant, the spectra exhibit certain shoulders. In this case, the spectra with shoulders could be understood as exchange-amalgamation of two different signals due to trapped and mobile solitons, where weak shoulders may originate from the trapped soliton signals with broader linewidth. Saturation study again showed no evidence for overlapping two kinds of lines, thus suggesting a rather strong exchange coupling of broad and narrow components due to trapped and mobile species, respectively. This point will also be discussed later.

By heating the sample above the temperature of approximately 215 K, the first-order phase transition into the AV state takes place, accompanied by a clear line broadening as shown in Fig. 2. The ESR line shape at 220 K is inhomogeneous by the overlap of the spectra at the low-temperature ACP state and the AV state above the ACP state, because the first order phase transition is not complete around this temperature. The line shape well above the transition temperature again becomes close to Lorentzian.

In order to examine the origin of the observed spins as Pt^{3+} species, we have measured the angular dependence of the g-value at various temperatures as shown in Fig. 3. The anisotropy of the g-value is well-described by the conventional expression as follows:[58]

$$g(\theta) = (g_{\parallel}^2 \cos^2\theta + g_{\perp}^2 \sin^2\theta)^{1/2}. \quad (1)$$

Here θ shows the angle between the chain axis and the external magnetic field. $g_{\parallel}$ and $g_{\perp}$ show the principal g-values parallel and perpendicular to the chain axis, respectively. Solid and dashed lines show the fitting curves according to Eq. (1) for the data at 280 and 364 K, respectively. Observed values of $g_{\parallel}$ and $g_{\perp}$ are 1.970 and 2.211, respectively, at 280 K. These values agree well with those reported for low-spin Pt^{3+} ions.[59] In addition, the observed anisotropy of the $g11$-values, $g_{\perp} > 2 > g_{\parallel}$, agrees well with the result of the crystal-field calculation for the Pt^{3+} ion with the unpaired electron residing in the Pt($5d_{z^2}$) orbital;[60]

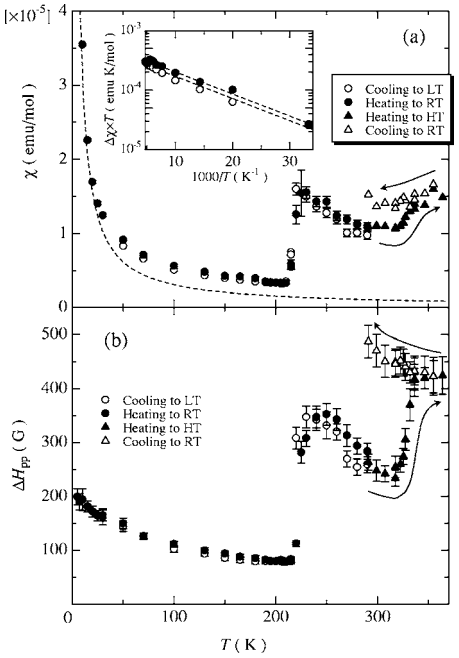

FIG. 4. Temperature dependence of (a) the spin susceptibility χ and (b) peak-to-peak ESR linewidth, ΔH_{pp}, with H perpendicular to the chain axis. The data for higher temperatures than room temperature are obtained after measuring the data of low temperatures. The dashed line in (a) represents the fitting curve by the Curie-law. Arrows are guides to the eyes. Inset of (a) represents the temperature dependence of the thermally activated component obtained by subtracting the Curie-component from the observed χ, see text for details. Dashed lines for open and closed circles are fitting lines for cooling and heating, respectively.

$$g_{\perp} = 2 - 6(\lambda/\Delta) - 6(\lambda/\Delta)^2 > 2,$$

$$g_{\parallel} = 2 - 3(\lambda/\Delta)^2 < 2. \quad (2)$$

Here Δ and λ denote the crystal-field splitting energy between d_{z^2} and $d_{yz,zx}$ orbitals and spin-orbit coupling constant ($\lambda < 0$), respectively. The g-values exhibit a slight increase when the crystal phase is transformed into the HT phase for $T > 324$ K, implying the modification of Δ associated with the phase transition at 324 K.

Figure 4 shows the temperature dependence of (a) spin susceptibility χ and (b) peak-to-peak width of the first-derivative ESR spectrum ΔH_{pp} with H perpendicular to the chain axis. Two anomalies observed both in χ and ΔH_{pp} around 215 and 324 K are caused by the structural phase transitions between the LT and RT phases and between the RT and HT phases, respectively. A drastic decrease of χ around 215 K is consistent with the formation of the nonmagnetic ACP state in the LT phase, as reported previously.[36]

In the temperature range below about 20 K of the ACP state, χ obeys the Curie law as drawn by the dashed curve in Fig. 4(a). The spin concentration N_s determined from χ gives 6.7×10^{-4} spins per Pt-Pt-I unit. The origin of the Curie component may be ascribed to the isolated Pt^{3+} ions created at the chain ends or defect sites. A prominent feature is that, with increasing temperature, the spin concentration begins to

show an enhancement from the Curie component χ_c. The enhanced component $\Delta\chi(\equiv\chi-\chi_c)$ is well-described by the activation formula, that is, $\Delta\chi\propto(1/T)\exp(-E_g/k_BT)$ as shown in the inset of Fig. 4(a). The activation energy E_g is estimated to be about 90 K. In addition, ESR linewidth shown in Fig. 4(b) exhibits clear narrowing with increasing temperature, associated with the change of the line shape from a nearly Gaussian to Lorentzian as shown in Fig. 2. These results agrees well with our previous report,[36] which suggests that the activated spins exhibit a thermal motion. We have proposed that such a mobile spin is the kink between the degenerate valence-ordering states of the ACP state, that is, $[\cdots Pt^{2+}\text{-}Pt^{3+}\text{-}I^{-}\text{-}Pt^{3+}\text{-}Pt^{2+}\cdots]$ and $[\text{-}Pt^{3+}\text{-}Pt^{2+}\cdots I^{-}\cdots Pt^{2+}\text{-}Pt^{3+}\text{-}]$, similar to the soliton-kink in the *MX*-chain complexes.[8,26] The existence of the soliton-kink in *MMX*-chains has also been predicted theoretically.[46,47] Further evidence for the motion of the spins is given later from the discussion of angular dependence of the motionally narrowed linewidth in the ACP state in Sec. IV B.

In the AV state consisting of the RT and HT phases, a clear increase of χ from those of the ACP state is observed. In this case, the dominant contribution of observed χ would be originating from the delocalized conduction-electron spins, the presence of which is expected from the good electrical conductivity in the AV state.[35,38] The presence of the Q1D conduction-electron system is also discussed later from the angular dependence of the ESR linewidth, which probes the spin dynamics.

Around the transition temperature of 324 K between the RT and HT phases, a hysteretic behavior is observed. Once the system is heated up to the HT phase, both χ and ΔH_{pp} do not return to their RT values even though the samples are cooled down to room temperature. We heated the samples again after cooling down to room temperature, but observed no anomalies around 324 K in this thermal process. Such behavior is also observed in the transport properties and calorimetric studies.[35,41] Furthermore, the Curie spin concentration in the LT phase is also affected once the HT phase is formed, that is, it increases by nearly an order of magnitude larger than that obtained from the measurement cooled directly from the RT phase. Since the Curie component may arise either from the chain ends or defect states, the increase of this component may indicate the occurrence of a kind of scission of the 1D chain at the structural phase transition from the RT to HT phase. In fact, we have observed a remarkable broadening of the ESR linewidth around 324 K, which may be related to the increased scattering rate of the conduction electron due to the increase of the Curie component reflecting the number of defect concentration, as to be discussed in Sec. IV A.

As pointed in Sec. I, the anisotropy of the ESR linewidth crucially probes the spin dynamics of the Q1D system.[52,54,57] The angular dependence of ΔH_{pp} is shown in Fig. 5(a) for the ACP state and (b) for the AV state. As seen in this figure, the angular dependence of ΔH_{pp} is markedly different between the ACP and AV states. Figure 5(a) shows the angular dependence of ΔH_{pp} in the nonmagnetic ACP state, where the spin-spin interaction is negligible due to the dilute concentration of the spins. In this case, the hyperfine interaction would be expected to be the dominant contribution to the

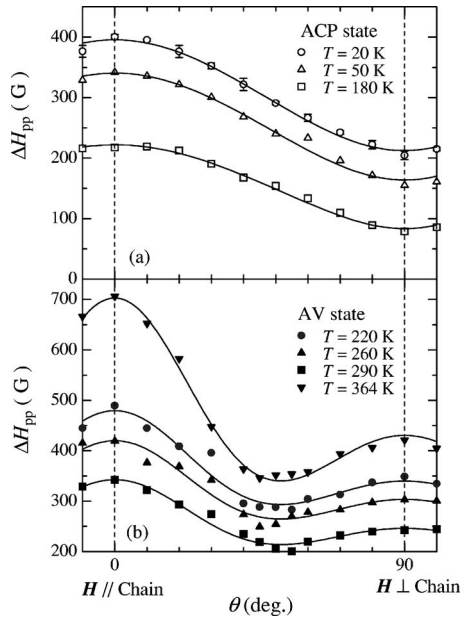

FIG. 5. Angular dependence of peak-to-peak linewidth, ΔH_{pp}, in (a) the ACP state at low temperatures and (b) the AV state for both the RT and HT phases. The solid curves in (a) represent the guides to the eyes, whereas those in (b) are least-squares fitting results by Eq. (3).

linewidth.[36] This is reasonably supported by the fact that the linewidth shows a uniaxial anisotropy with the maximum being observed for H parallel to the chain. This is consistent with the uniaxial anisotropy of hyperfine interaction due to Pt and I nuclear spins, similar as in the case of the Pt-Cl-chain complex.[61] Based on the motional narrowing theory, the spin dynamics associated with the motion of the thermally activated soliton is discussed further from the anisotropic properties of ΔH_{pp} in the next section.

On the other hand, a clear minimum of ΔH_{pp} is observed around 50° in the AV state, both in the RT and HT phases as shown in Fig. 5(b). The appearance of this minimum can be regarded as the direct evidence of the formation of the Q1D conduction-electron system in this material, as mentioned in Sec. I. That is, the secular component of the spin-spin dipolar-interaction dominates the motionally narrowed dipolar-width in the Q1D system, exhibiting a power-law relation of the $\{3(g_\parallel/g)^2\cos^2\theta-1\}$ for its angular dependence of the linewidth. Here g shows the angular-dependent g-value given by Eq. (1). Then the linewidth would exhibit a minimum around the magic angle θ_m ($\theta_m=51.6°$ by using the experimentally obtained g-values). On the other hand, observed nonzero value of ΔH_{pp} even at θ_m clearly indicates the other contribution to the linewidth, that is, the spin-phonon relaxation component $T_2^{s\text{-}ph}$ similar to the cases of some TCNQ salts and KCP.[53,54] By considering that the total linewidth is described by the superposition of spin-spin and spin-phonon relaxation components as $1/T_2=1/T_2^{s\text{-}s}+1/T_2^{s\text{-}ph}$, we find that the observed angular dependence of ΔH_{pp} in the AV state is well fitted by the following phenomenological equation, as shown by the solid curves in Fig. 5(b):

$$\Delta H_{pp}(\theta) = A + B\{3(g_{\parallel}/g)^2 \cos^2\theta - 1\}^2. \quad (3)$$

Here A and B represent the contributions of $1/T_2^{s\text{-}ph}$ and $1/T_2^{s\text{-}s}$, respectively. Since we could not find additional angular-dependent components to $\{3(g_{\parallel}/g)^2 \cos^2\theta - 1\}^2$, we assume that the angular dependence of A is negligibly small compared with that of the second term in the right-hand side of Eq. (3). The square power dependence of the secular term $\{3(g_{\parallel}/g)^2 \cos^2\theta - 1\}$ results from the Q1D nature of the present system with finite interchain coupling, similar as observed in the case of KCP. From the obtained magnitudes of parameters A and B, we discuss the spin dynamics of the conduction electron based on the ESR theory of Q1D conductors in the next section.[52,54]

IV. DISCUSSIONS

In this section, we first discuss the spin dynamics of the AV states consisting of the RT phase between 215 and 324 K and the HT phase above 324 K. In both phases, ESR linewidth shows clear anisotropies due to the secular dipolar term, as described in the previous section. Q1D spin dynamics is confirmed from the observed secular dipolar anisotropies proportional to the square of the secular term, that is, $\{3(g_{\parallel}/g)^2 \cos^2\theta - 1\}^2$ as mentioned in Sec. I. In addition, the observed Lorentzian line shape also provides evidence for the presence of interchain spin hopping as discussed in the Q1D system in comparison with the pure 1D system that exhibits the line-shape intermediate between Lorentzian and Gaussian.[52,56,57] Next we discuss the motional narrowing effect of the ESR spectra of thermally excited solitons based on the motional narrowing theory, by focusing on its anisotropic behavior through the expression of ω_p^2/ω_e.

A. Spin dynamics of the conduction electron in the AV state—Evidence for the Q1D conductor

It has been shown that the ESR linewidth in Q1D conductors is given by the superposition of the spin-phonon and spin-spin contributions as $1/T_2 = 1/T_2^{s\text{-}s} + 1/T_2^{s\text{-}ph}$. Here T_2 shows the total relaxation time and $T_2^{s\text{-}s}$ and $T_2^{s\text{-}ph}$ show the spin-phonon and spin-spin relaxation times, respectively. As mentioned in preceding sections, the latter term governs the observed characteristic angular variation. In this section, we discuss the magnitude and its temperature dependence of these terms more specifically and relate them to the property of Q1D conduction-electron systems in the relevant electronic phases.

1. Spin-spin relaxation

In this section, we discuss the spin-spin relaxation, as determined from the observed magnitude of the linewidth component that shows the characteristic angular variation of the secular dipolar term. Tomkiewicz *et al.* have shown that the significant contribution of the spin-spin relaxation in Q1D conductors results from the relative suppression of spin-phonon relaxation due to the restriction of the spin-flip scattering of the conduction electrons in the Q1D system, as mentioned in Sec. I.[52,53] In fact, they have shown that some charge transfer salts of TTF-halides exhibit a significant contribution of spin-spin dipolar relaxation in the linewidth. They have applied the discussion of the Q1D Heisenberg spin system to estimate the observed magnitude of dipolar width. Due to the presence of interchain hopping in the Q1D system, the resultant ESR spectrum becomes as a Lorentzian with its half-width η described as[49,52]

$$\eta \sim \langle \Delta\omega^2 \rangle (\tau_{\parallel}\tau_{\perp})^{1/2}. \quad (4)$$

Here, $\langle \Delta\omega^2 \rangle$ denotes the secular dipolar second moment. $\tau_{\parallel}$ and $\tau_{\perp}$ show the intrachain and interchain hopping time, respectively. Then $(\tau_{\parallel}\tau_{\perp})^{1/2}$ becomes the effective hopping time for the linewidth narrowing.

While this equation has been employed to semiquantitatively explain the dipolar contribution in TTF-halides, no study was reported on the anisotropic properties by using single crystals to directly confirm whether the anisotropy is governed by the secular dipolar term expected for Q1D spin systems. Then Takahashi *et al.* have successfully observed the secular dipolar anisotropy in their ESR studies of a Q1D conductor, KCP.[54] They have successfully explained the observed magnitude and the temperature dependence of the secular dipolar term by developing a theoretical framework based on the linewidth theory of Q1D Heisenberg spin chains by considering that the mean distance of spins may be determined by the carrier concentration. The conduction electrons in KCP are actually thermally activated carriers and not the conduction electrons of degenerate conductors within the temperature range of their work. Yet the expression for the secular dipolar width due to conduction electron spins may be equally applicable to the case of a degenerate conductor where the carrier concentrations are considered to be nearly temperature independent. So, we adopt their expression shown below for the discussion of dipolar width in the present system as the first approximation. The linewidth η in this case may be given by the following expression.[54]

$$\eta = \langle \Delta\omega_0^2 \rangle \{3(g_{\parallel}/g)^2 \cos^2\theta - 1\}^2 (\tau_{\parallel}\tau_{\perp})^{1/2} P. \quad (5)$$

Here P represents the probability that a spin finds another spin on the neighboring sites. This factor is equivalent to the density of the conduction electron n by assuming the random distribution of the conduction electron on the chain, which should be less than unity. $\langle \Delta\omega_0^2 \rangle$ is defined as the secular-dipolar second moment for the one-dimensional spin arrangement without its angular dependent part and is given by the following equation.[54,58]

$$\langle \Delta\omega_0^2 \rangle = \frac{1}{\hbar^2} \frac{S(S+1)}{3} \left(\frac{2g_{\parallel}^2 + g_{\perp}^2}{2} \beta^2 \right)^2 l_c^{-6}, \quad (6)$$

where β and l_c represent the Bohr magneton and the nearest-neighbor spin-spin distance corresponding to the lattice constant along the chain axis, respectively. If we further define $\langle \Delta\omega_0^2 \rangle \equiv \omega_0^2$, and $(\tau_{\parallel}\tau_{\perp})^{1/2} \equiv 1/\omega_{ex}$ where ω_{ex} becomes an effective hopping frequency, the above equation can be expressed as

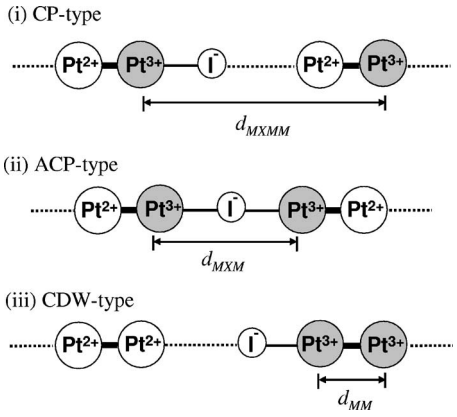

FIG. 6. Schematic illustrations of the valence configuration formed when the two conduction electrons encounter each other. (i) the CP-type configuration, (ii) the ACP-type configuration, and (iii) the CDW-type configuration. Thin-solid and broken lines represent the shorter and longer Pt–I distances, respectively, whereas the thick lines represent the Pt–Pt bonds. The nearest-neighbor Pt^{3+}-Pt^{3+} distances are also shown as d_{MXMM}, d_{MXM}, and d_{MM} for (i), (ii) and (iii), respectively.

$$\eta = \omega_0(\omega_0/\omega_{ex})P\left(3\frac{g_{\parallel}^2}{g^2}\cos^2\theta - 1\right)^2. \quad (7)$$

This expression can be compared with the experimentally observed angular dependence of Eq. (3) given in Sec. III. It can be seen that $(\omega_0/\omega_{ex})P$ gives the effective reduction factor of the motional narrowing of the static linewidth, ω_0. To go further we need to estimate the secular dipolar second moment which can be calculated based on the nearest-neighbor spin arrangements in the possible valence state of the *MMX*-chain.

Owing to the bimetal backbone bridged by a halogen, three types of the valence configuration are considered for the two conduction electrons to encounter each other on a chain as illustrated in Fig. 6. These configurations provide the nearest-neighbor distance l_c in Eq. (6). They are (i) the CP-type valence configuration where l_c becomes the unit repetition distance, d_{MXMM}; (ii) the ACP-type configuration where l_c is the Pt^{3+}-I^--Pt^{3+} distance via bridged I^- ion, d_{MXM}; and (iii) the CDW-type configuration with l_c corresponding to the direct Pt^{3+}-Pt^{3+} distance within a Pt dimer, d_{MM}. From the structural analyses at 253 K shown in Fig. 1, the following distances can be obtained for the RT phase: d_{MXMM} =8.590 Å (Pt1-Pt3), d_{MXM}=5.917 Å (Pt2-Pt3), and d_{MM} =2.673 Å (Pt1-Pt2).[35]

From these parameters, the half width at half height of the static ESR spectrum is calculated from the square-root of the second moment in the frequency unit. The calculated values are compared with the experimental parameters *B* obtained from ΔH_{pp} by multiplying the factors $(2/\sqrt{3})(\hbar/g\beta)$ for a Lorentzian line shape.[62] In the limit of *P* being unity, which provides the upper limit of the dipolar linewidth for the given l_c-values in Fig. 6, the dipolar linewidth is calculated as 34, 74, and 803 G for the configurations (i), (ii), and (iii), respectively. Experimentally observed dipolar linewidth (*B*-term) is shown in Fig. 7 together with the *A*-term. As seen

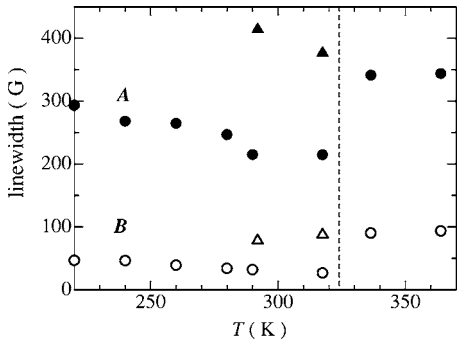

FIG. 7. Temperature dependence of the *A*-term, the spin-phonon relaxation component (solid symbols) and the *B*-term, the spin-spin relaxation component (open symbols) obtained by the least-squares fitting of the angular dependence of the ESR linewidth by Eq. (3). Closed and open triangles represent the data down to room temperature after the monotropic phase transition to the HT phase has taken place. Dashed line represents the transition temperature from the RT phase to the HT phase (324 K) (Ref. 41).

in this figure, the magnitude of the *B*-term varies from 46 G at 240 K to 27 G at 320 K in the RT phase.

It is immediately recognized that the most probable valence configuration to provide the observed large dipolar linewidth is (iii), CDW configuration because the other two configurations give only the same order of magnitude with the experimental observation. When the experimentally observed dipolar width is described by Eq. (7), the reduction factor of the observed dipolar width from the calculated dipolar width is given by $(\omega_0/\omega_{ex})P$ as discussed above. We can check whether this expression is compatible with the observed value. If we adopt the case of (iii), the reduction factor becomes $27/803 \sim 0.04$ at 320 K, for example. Although the exact value of *P* is not known, an order estimation may be possible when we consider that the concentration of the conduction electrons that can make spin flip is roughly given by k_BT/W due to Fermi statistics. Here k_BT represents the fraction of conduction electrons that can make spin flip against the total carrier population represented by the bandwidth *W*. At RT, $k_BT \sim 300$ K (0.03 eV) would give the order of $P \sim k_BT/W \sim 0.01$, if *W* be several eV due to a relatively narrow bandwidth. By adopting this value for *P*, the above ratio of 0.04 for $(\omega_0/\omega_{ex})P$ gives ω_0/ω_{ex} close to unity. Such a situation, however, may not be consistent with the physical process of motional narrowing that involves averaging the static dipolar width by spin flip, giving Lorentzian line shape, that would require at least $\omega_0/\omega_{ex} \lesssim 0.1$.

One possible explanation would be the presence of localized defect spins (or Curie-type spins) that can interact with conduction-electron spins. Fine structures of such defect spins, if any, may be washed out by a spin exchange between the conduction electron spin and the localized spin to give the observed width. One candidate is the $S=1$ defect state similar to those observed in another series of *MMX*-chain compounds of $A_4[Pt_2(pop)_4I]\cdot nH_2O$ (A =Li, Na, K, Rb, Cs; pop=$P_2O_5H_2^{2-}$) as evidenced from the observation of a $g \sim 4$ line.[30] $S=1$ defect site may be created, for example, at lattice imperfection such as a scission of the Pt–I bond, that may cause the elongation of the adjacent

Pt–Pt bond, resulting in the formation of $S=1$ with parallel spins of Pt^{3+}-Pt^{3+} pair. Isolated $S=1$ state in the uniaxial case is characterized by the doublet fine structure due to the zero-field splitting of the secular type represented by $D\{3(g_{\parallel}/g)^2\cos^2\theta-1\}^2$ due to the DS_z^2 term in the spin Hamiltonian accompanied by the $g\sim 4$ line of so-called forbidden transition. The magnitude of D is determined by the spin-spin dipolar interaction. When there are exchange interactions between spins, the doublet structure tends to be washed out and the more stronger the exchange interaction, the weaker the intensity of the $g\sim 4$ line as observed in the above $A_4[Pt_2(pop)_4I]\cdot nH_2O$ compounds.[30] If such a $S=1$ state interacts with Q1D conduction-electron spins, the overall linewidth may be again determined by the secular-type dipolar anisotropy, which at least does not contradict with the observed secular-type anisotropy in the present Q1D *MMX*-conductor.

At present, the numerical estimation of the spin concentration of such $S=1$ spin defects is difficult. It should be pointed out, however, that the contribution to the overall spectra of the conduction electron spin is not negligible at all compared with the defect spins. This becomes clear when one considers that the secular term, $\{3(g_{\parallel}/g)^2\cos^2\theta-1\}^2$, becomes zero at the magic angle, while the linewidth has finite value at this angle for all of the temperature region of the AV state, represented by the A-term in Eq. (3). This contribution cannot arise either from the secular-dipolar term of the conduction electron or the above-mentioned $S=1$ state and should be attributed to the contribution of spin-phonon relaxation, $T_2^{s\text{-ph}}$ of the Q1D conduction electron spin. In the next section we will discuss the origin of this spin-phonon term together with its temperature dependence.

2. Spin-phonon relaxation

In the conducting state, the spin-phonon component is governed by the spin-flip scattering of the conduction electron through the spin-orbit coupling, known as Elliot mechanism.[55] This mechanism predicts the angular dependence of linewidth similar to g-value anisotropy, typically observed in many 1D or Q1D organic conductors.[63,64] On the other hand, the angular dependence of the spin-phonon contribution is practically negligible in the present system, as shown in Fig. 5(b), where the angular dependent linewidths are fitted by Eq. (3). This could be related to the fact that in many 1D or Q1D organic conductors with good conductivities, the linewidths are much sharper and not accompanied by dipolar contribution, which may bring observable anisotropy for the spin-phonon contribution. To understand the relatively large linewidths and their weak angular dependence here would require more theoretical work of the present platinum complex that is expected to exhibit a much stronger electron correlation effect as compared with typical organic conductors.[43] It should be also pointed out that similar behavior of ESR linewidth anisotropy given by Eq. (3), that is, prominent dipolar term and practically angular independent spin-phonon term, is reported in another typical platinum conductor, KCP.[54]

As for the temperature dependence of the spin-phonon component due to the Elliot mechanism, it is well-known that $1/T_2^{s\text{-ph}}$ is proportional to $1/\tau_R$, where τ_R represents the scattering time. In other words, the ESR linewidth becomes proportional to the electrical resistivity, that increases as increasing temperature. In the present complex, however, the temperature dependence of the A-term is opposite to the behavior expected for the Elliott mechanism which is prominent in the RT phase as shown in Fig. 7. That is, the observed value decreases with increasing temperature, opposite to the electrical resistivity that exhibits a positive temperature coefficient above 240 K.[35] Such an anomalous behavior of $T_2^{s\text{-ph}}$ has been observed in some Q1D conductors such as TTF-TCNQ and HMTTF-TCNQ.[53] In these materials, it is reported that the spin-flip scattering process is governed by the $2k_F$ Peierls fluctuation of the lattice, which does not necessarily coincide with the overall electron scattering causing the electrical resistivity because the scattering of the conduction electron is spin-independent.[53] In this case, the fluctuation amplitude and its correlation length increase with decreasing temperature as approaching the Peierls transition temperature. Then, the scattering rate becomes greater with decreasing temperature, which causes the line-broadening of the ESR spectrum for low temperatures.

A similar situation may occur in the present case of $Pt_2(n\text{-pentylCS}_2)_4I$, where the x-ray diffuse scattering due to a twofold lattice fluctuation has been observed both in the RT and HT phases,[35] that are well above the transition temperature to the ACP state of 207 K.[41] Thus the temperature dependence of the A-term might be explained by the shortening of the $T_2^{s\text{-ph}}$ as the temperature approaching the transition temperature between the RT and LT phases due to the spin-flip scattering of the conduction electron by the reported twofold lattice fluctuation of *MMX*-units.

In the HT phase, the scattering of conduction electrons by defect sites is seen to be more prominent, as can be recognized from an abrupt increase of the A-term. This increase may be reasonably ascribed to the increase of the Curie spin concentration in the HT phase, as pointed out in Sec. III. Correspondingly, the B-term also abruptly increases at the phase transition temperature. This is also reasonable from the discussion of the previous section that the magnitude of B is governed by the spectral weight of defect spins, which should become larger at the HT phase. When we lower the temperature below the transition temperature of 324 K after the monotropic transition to the HT phase has taken place, the magnitudes of both the A- and B-terms retain their values at the HT phase as shown in Fig. 7. This phenomenon also supports that the linewidth reflects the intrinsic nature of the electronic phases of the present system. It should be pointed out that the A-term also exhibits a clear increase as the temperature approaching transition temperature to the ACP phase, similar as in the RT phase. This again supports the interpretation that the temperature dependence of the A-term is sensing the thermal fluctuation of the lattice system.

B. Spin dynamics of the thermally activated solitons in the ACP state

As already mentioned, the nonmagnetic and insulating ACP state is formed in the present system below about

215 K, where the drastic change of the ESR signals occurs as described in Sec. III. In the ACP state, the spin susceptibility obeys Curie-law below about 20 K. On the other hand, above 20 K it exhibits an enhancement from the Curie-law with a finite activation energy of 90 K as shown in Fig. 4(a). At the same time, ESR linewidth exhibits an enhanced narrowing as the temperature is raised [Fig. 4(b)], accompanied by a change of the line shape from Gaussian to Lorentzian (Fig. 2). These results agree well with our previous measurements,[36] suggesting that the thermally activated spins are the solitons in the ACP state. In our previous paper, however, only the data for H perpendicular to the chain were presented. In this section, we discuss the motional narrowing of the ESR linewidth due to the mobile solitons from the angular dependence of the linewidth.

In the angular dependence of ΔH_{pp} in Fig. 5(a), the magic angle due to the dipolar interaction observed in the AV state is completely absent in the whole temperature range of ACP state. This result shows the absence of spin-spin dipolar interaction, which is consistent with the fact that the spin concentration is quite small in the ACP state of the order of 10^{-4} spins per *MMX* unit. In this case, the origin of the linewidth in the very low-temperature region may be reasonably ascribed to unresolved hyperfine (hf) and superhyperfine (shf) interactions caused by the ^{195}Pt ($I=1/2$, natural abundance of 33.7%) and ^{127}I ($I=5/2$, 100%), similar to the diluted-spin case reported for an *MX*-chain complex of Pt-I, where the hf-originated ESR lines of the Pt^{3+} ions have been reported.[59] In the present case, the hf splitting is absent as shown in Fig. 2 in spite of the small spin concentration. However, when a spin is shared by several atoms, the linewidth becomes unresolved due to the static distribution of individual hf lines. In such a situation, the hf splitting contributes to the overall ESR linewidth, as observed in the above-mentioned *MX*-chain of Pt-I.[59] In this case, the total span (or wing span) of a nearly Gaussian-shaped resonance line H_{span}, shown in Fig. 2, is unchanged regardless of the spin delocalization length under the static spin distribution.[5] We defined the H_{span} to be the separation between the magnetic fields where the absolute value of the first-derivative ESR signal intensity reduces to 1% of those of the peak fields. The obtained value for 4 K is about 1000 G, which is almost the same amplitude as that of the Pt-I chain ($\sim$1000 G), indicating that the spin distribution is almost static.

In this respect, the angular distribution of the linewidth provides a crucial probe for further examining the hyperfine-determined linewidth and its temperature-dependent motional narrowing effect. The hyperfine tensors of either Pt or bridging I are expected to show uniaxial anisotropies with respect to the *MMX*-chain axis, due to their d_{z^2} or p_z orbitals, respectively, both of which are pointing parallel to the chain axis. That is, $A_{\parallel}>A_{\perp}$, which should bring about similar uniaxial anisotropy for the resultant unresolved hyperfine-determined ESR linewidth. In fact, the observed linewidth shows a clear uniaxial anisotropy with larger width parallel to the chain axis, that is, $\Delta H_{\mathrm{pp}\parallel}>\Delta H_{\mathrm{pp}\perp}$, as shown in Fig. 5(a), further providing evidence that the observed ESR linewidth is determined by unresolved hyperfine structures.

From the above discussions, the second moment of the hyperfine-determined linewidth may be written as ω_{p}^2, and hence ω_{p} gives the observed linewidth in the static limit. When the motional narrowing takes place with the hopping frequency of ω_{e}, the resultant linewidth is given as $\omega_{\mathrm{p}}^2/\omega_{\mathrm{e}}$ under the extreme narrowing condition of $\omega_{\mathrm{p}}\ll\omega_{\mathrm{e}}$. Since the hopping of thermally excited solitons occurs primarily along the chain axis, ω_{e} may be regarded as the effective hopping frequency analogous to that given in the previous section within the framework of Q1D spin dynamics. Thus the motional effect changes the dependence of the linewidth on ω_{p}, from the linear dependence of ω_{p} for the static limit to the square dependence of ω_{p}^2 for the extreme narrowing. Then the ratio $\Delta H_{\mathrm{pp}\parallel}/\Delta H_{\mathrm{pp}\perp}$ crucially probes the occurrence of motional narrowing by examining whether the anisotropy ratio varies from the linear dependence of $\omega_{\mathrm{p}\parallel}/\omega_{\mathrm{p}\perp}$ to approach the square dependence of $(\omega_{\mathrm{p}\parallel}/\omega_{\mathrm{p}\perp})^2$ as the narrowing becomes more evident for higher temperatures. Here ω_{p} exhibits the uniaxial anisotropy of $\omega_{\mathrm{p}\parallel}>\omega_{\mathrm{p}\perp}$ due to the above-mentioned hyperfine and superhyperfine couplings. In this context, one complication should be considered in relating the anisotropy of the static coupling, $\omega_{\mathrm{p}\parallel}/\omega_{\mathrm{p}\perp}$ to the anisotropy of the observed peak-to-peak linewidth, $\Delta H_{\mathrm{pp}\parallel}/\Delta H_{\mathrm{p}\perp}$, when the ESR spectra exhibit weak shoulders which reflect the existence of exchange-coupled two kinds of spin species with different linewidths. As mentioned in Sec. III the saturation study of the spectra at 20 K$<T<$180 K did not show any changes of the relative intensity of side peaks, which strongly suggests that the narrow- and broad-linewidth species are exchange-coupled and that the former and the latter species are likely to be thermally excited spins and Curie spins, respectively. In the ESR spectra of such exchange-coupled spin system of different linewidths, it is well-known that the linewidths of individual components are more appropriately estimated from the corresponding components as far as these individual structures are recognized in the spectral line shape.[65] Thus we adopt the peak-to-peak linewidth, ΔH_{pp} of the whole spectra, as representative of narrow species, that is, the thermally excited mobile solitons. This is a kind of first approximation to qualitatively discuss the occurrence of motional narrowing phenomenon through the linewidth anisotropy.

Figure 8(a) shows the temperature dependence of the peak-to-peak linewidth normalized by the value at 4 K with the external magnetic field perpendicular to the chain axis, which shows the degree of motional narrowing. Figure 8(b) shows the temperature dependence of the anisotropy of the observed peak-to-peak linewidth, $\Delta H_{\mathrm{pp}\parallel}/\Delta H_{\mathrm{pp}\perp}$. The lower and upper dotted lines show the values of $\omega_{\mathrm{p}\parallel}/\omega_{\mathrm{p}\perp}$ and $(\omega_{\mathrm{p}\parallel}/\omega_{\mathrm{p}\perp})^2$, respectively, the former being set equal to $\Delta H_{\mathrm{pp}\parallel}/\Delta H_{\mathrm{pp}\perp}$ at 4 K and the latter obtained by squaring it. It is seen that the static value at 4 K increases and tends to approach its square, although the highest value of 2.8 at 180 K is not as high as the limiting value of 3.9, given by the upper dotted line. This lower value than 3.9 may be reasonable, if we consider that the normalized linewidth of about 0.4 is still considerably larger than the value at the extreme narrowing condition of less than 0.1, which suggests that the narrowing is not yet complete. Thus the gradual increase of $\Delta H_{\mathrm{pp}\parallel}/\Delta H_{\mathrm{pp}\perp}$ as the temperature increases strongly suggests the occurrence of the motional narrowing of the ESR spectra for higher temperatures.

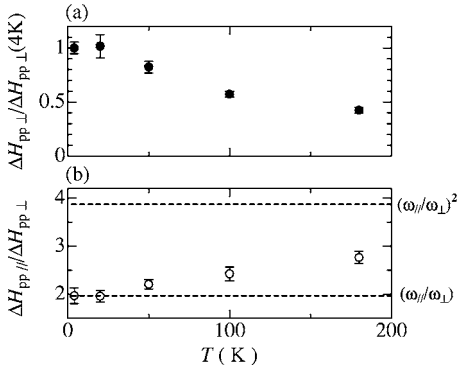

FIG. 8. Temperature dependence of (a) peak-to-peak linewidth normalized by the value at 4 K with the external magnetic field perpendicular to the chain axis, and (b) the anisotropy of the observed peak-to-peak linewidth, $\Delta H_{pp\parallel}/\Delta H_{pp\perp}$. The lower and upper dotted lines in (b) represent the value of $\omega_{p\parallel}/\omega_{p\perp}$ and $(\omega_{p\parallel}/\omega_{p\perp})^2$, respectively. See text for details.

Finally, it should be pointed out that the observed ESR spectral line shape at 4 K may provide a unique probe for studying the detailed shape of spin distribution of the soliton. This situation, of course, stands for the case when the observed immobile spins at 4 K can be regarded as the trapped soliton, which may be possible. This is because the ESR spectra exhibit slight linewidth narrowing, indicating the spin motion even below 20 K where the thermal excitation of the soliton is negligible, as can be seen from Fig. 4(b). As discussed above, the observed ESR linewidth at 4 K and hence the line shape of these spins are reasonably ascribed to the unresolved hf and shf structures. Then the nearly Gaussian line shape with slightly flat peaks, shown in Fig. 2, would reflect the specific spin distribution functions. In this context, the simulation of hf-originated ESR spectra may provide us the experimentally determined wave function of the soliton in the present *MMX*-chain complex. Such a simulation work would be an interesting problem which requires the theoretical distribution function[4,5] and is left open for further studies. The other interesting feature related to soliton is the reversed spin-charge relationship, which has been typically elucidated in the case of the soliton in polyacetylene.[4] That is, the neutral soliton with spin $S=1/2$ does not possess charge, i.e., $Q=0$. Such confirmation could be done, for example, by studying the correlation between the light-excited ESR signal, probing the photoexcited spins, and the photocurrent, probing the photoexcited charges.[66] Thus the spin-charge relationship would also be an interesting problem left for further inquiries.

V. CONCLUSIONS

ESR measurements have been carried out on single crystals of a quasi-one-dimensional *MMX*-chain complex of $Pt_2(n\text{-pentylCS}_2)_4I$ which exhibits successive electronic phase transitions. Principal g-tensor components obtained are $g_\parallel=1.970$ and $g_\perp=2.211$, where $g_\parallel$ and $g_\perp$ represent the g-component parallel and perpendicular to the chain axis, respectively. These values are consistent with those of Pt^{3+} ions in the low-spin state, i.e., $S=1/2$.

The anisotropy of the ESR linewidth has shown a drastic change around 215 K where the phase transition takes place between the nonmagnetic alternate-charge-polarization (ACP) state for low temperatures and the paramagnetic averaged-valence (AV) state with a relatively good electrical conductivity for higher temperatures. In the AV state, consisting of the room-temperature (RT) phase below 324 K and the high-temperature (HT) phase above this temperature, the ESR linewidth shows a clear minimum at the magic angle of about 50° from the chain direction due to the secular dipolar term, representing the spin-spin relaxation, $T_2^{s\text{-}s}$. The linewidth also exhibits a nearly angular independent component representing the spin-phonon relaxation, $T_2^{s\text{-}ph}$. The observed feature is consistent with those reported previously for a Q1D conductors such as charge transfer salts and Pt-complexes, providing microscopic evidence for the occurrence of a Q1D conduction-electron system in the present *MMX*-chain complex.

In the ACP state, the spin concentration drastically decreases due to the nonmagnetic nature of the background electronic state. The ESR linewidth shows a uniaxial anisotropy with respect to the chain axis, which can be reasonably ascribed to the unresolved hyperfine structures due to Pt and iodine nuclear spins. The spin susceptibility shows a clear enhancement from Curie-type behavior above 20 K, accompanied with a gradual change of the line shape from Gaussian to Lorentzian with motional narrowing as the temperature is raised. The observed spins are conjectured to be thermally excited solitons. The motional narrowing effect is further confirmed from the anisotropic behavior of the linewidth; a linear dependence on the static hyperfine width ω_p at low temperatures gradually approaches to ω_p^2-dependence at higher temperatures, according to the framework of the motional narrowing theory of ω_p^2/ω_e where ω_e represents the effective frequency of Q1D spin motion. The observed ESR line shape at 4 K at the same time provides the basis for analyzing the spin density distribution of the soliton through the study of the hyperfine coupling governed by the static spin distribution, which may be approached by further theoretical studies.

ACKNOWLEDGMENTS

The authors express their gratitude to Professor H. Ito, Dr. K. Marumoto, Professor K. Saito, and Professor H. Kitagawa for valuable discussions. This work has been partially supported by Grant-in-Aid for Scientific Research (17740191 and 17340094) and for Science Research in a Priority Area "Super-Hierarchical Structures" (17067007) from the Ministry of Education Culture, Sports, Science and Technology of Japan.

[1] S. Kagoshima, H. Nagasawa, and T. Sambongi, *One-Dimensional Conductors* (Springer-Verlag, Berlin, 1988).
[2] *Extended Linear Chain Compounds*, edited by J. S. Miller (Plenum, New York, 1982).
[3] *Low Dimensional Cooperative Phenomena*, edited by H. J. Keller (Plenum, New York, 1974).
[4] A. J. Heeger, S. Kivelson, J. R. Schrieffer, and W.-P. Su, Rev. Mod. Phys. **60**, 781 (1988).
[5] S. Kuroda, Int. J. Mod. Phys. B **9**, 221 (1995).
[6] K. Nasu, J. Phys. Soc. Jpn. **52**, 3865 (1983); **53**, 302 (1984); **53**, 427 (1984).
[7] K. Toriumi, Y. Wada, T. Mitani, S. Bandow, M. Yamashita, and Y. Fujii, J. Am. Chem. Soc. **111**, 2341 (1989).
[8] H. Okamoto, K. Toriumi, T. Mitani, and M. Yamashita, Phys. Rev. B **42**, 10381 (1990).
[9] H. Okamoto and M. Yamashita, Bull. Chem. Soc. Jpn. **71**, 2023 (1998).
[10] C. Bellitto, A. Flamini, L. Gastaldi, and L. Scaramuzza, Inorg. Chem. **22**, 444 (1983).
[11] C. Bellitto, G. Dessy, and V. Fares, Inorg. Chem. **24**, 2815 (1985).
[12] M.-H. Whangbo and E. Canadell, Inorg. Chem. **25**, 1726 (1986).
[13] S. Jin, T. Ito, K. Toriumi, and M. Yamashita, Acta Crystallogr., Sect. C: Cryst. Struct. Commun. **45**, 1415 (1989).
[14] M. Yamashita and K. Toriumi, Inorg. Chim. Acta **178**, 143 (1990).
[15] N. Kimura, H. Ohki, R. Ikeda, and M. Yamashita, Chem. Phys. Lett. **220**, 40 (1994).
[16] H. Kitagawa, N. Onodera, T. Sonoyama, M. Yamamoto, M. Fukawa, T. Mitani, M. Seto, and Y. Maeda, J. Am. Chem. Soc. **121**, 10068 (1999).
[17] M. Yamashita, S. Miya, T. Kawashima, T. Manabe, T. Sonoyama, H. Kitagawa, T. Mitani, H. Okamoto, and R. Ikeda, J. Am. Chem. Soc. **121**, 2321 (1999).
[18] Y. Wada, T. Furuta, M. Yamashita, and K. Toriumi, Synth. Met. **70**, 1195 (1995).
[19] N. Kuroda, M. Sakai, Y. Nishina, M. Tanaka, and S. Kurita, Phys. Rev. Lett. **58**, 2122 (1987).
[20] H. Kishida, H. Matsuzaki, H. Okamoto, T. Manabe, M. Yamashita, Y. Taguchi, and Y. Tokura, Nature (London) **405**, 929 (2000).
[21] S. Iwai, M. Ono, A. Maeda, H. Matsuzaki, H. Kishida, H. Okamoto, and Y. Tokura, Phys. Rev. Lett. **91**, 057401 (2003).
[22] S. Takaishi, Y. Tobu, H. Kitagawa, A. Goto, T. Shimizu, T. Okubo, T. Mitani, and R. Ikeda, J. Am. Chem. Soc. **126**, 1614 (2004).
[23] M. Yamashita, T. Ishii, H. Matsuzaka, T. Manabe, T. Kawashima, H. Okamoto, H. Kitagawa, T. Mitani, K. Marumoto, and S. Kuroda, Inorg. Chem. **38**, 5124 (1999).
[24] K. Marumoto, H. Tanaka, S. Kuroda, T. Manabe, and M. Yamashita, Phys. Rev. B **60**, 7699 (1999).
[25] Y. Wakabayashi, N. Wakabayashi, M. Yamashita, T. Manabe, and N. Matsushita, J. Phys. Soc. Jpn. **68**, 3948 (1999).
[26] H. Tanaka, K. Marumoto, S. Kuroda, T. Manabe, and M. Yamashita, J. Phys. Soc. Jpn. **71**, 1370 (2002).
[27] S. Takaishi, H. Miyasaka, K. Sugiura, M. Yamashita, H. Matsuzaki, H. Kishida, H. Okamoto, H. Tanaka, K. Marumoto, H. Ito, S. Kuroda, and T. Takami, Angew. Chem., Int. Ed. **43**, 3171 (2004).
[28] K. Iwano, J. Phys. Soc. Jpn. **68**, 935 (1999).
[29] K. Iwano, Phys. Rev. B **69**, 045104 (2004).
[30] K. Marumoto, H. Tanaka, S. Kozaki, S. Kuroda, S. Miya, T. Kawashima, and M. Yamashita, Solid State Commun. **120**, 101 (2001).
[31] H. Matsuzaki, T. Matsuoka, H. Kishida, K. Takizawa, H. Miyasaka, K. Sugiura, M. Yamashita, and H. Okamoto, Phys. Rev. Lett. **90**, 046401 (2003).
[32] M. Mitsumi, T. Murase, H. Kishida, T. Yoshinari, Y. Ozawa, K. Toriumi, T. Sonoyama, H. Kitagawa, and T. Mitani, J. Am. Chem. Soc. **123**, 11179 (2001).
[33] M. Mitsumi, S. Umebayashi, Y. Ozawa, K. Toriumi, H. Kitagawa, and T. Mitani, Chem. Lett. (2002), 258.
[34] M. Mitsumi, K. Kitamura, A. Morinaga, Y. Ozawa, M. Kobayashi, K. Toriumi, Y. Iso, H. Kitagawa, and T. Mitani, Angew. Chem., Int. Ed. **41**, 2767 (2002).
[35] M. Mitsumi (unpublished).
[36] H. Tanaka, S. Kuroda, T. Yamashita, M. Mitsumi, and K. Toriumi, J. Phys. Soc. Jpn. **72**, 2169 (2003).
[37] H. Ito, Y. Hasegawa, H. Tanaka, S. Kuroda, M. Mitsumi, and K. Toriumi, J. Phys. Soc. Jpn. **72**, 2149 (2003).
[38] H. Tanaka, Y. Hasegawa, H. Ito, S. Kuroda, T. Yamashita, M. Mitsumi, and K. Toriumi, Synth. Met. **152**, 141 (2005).
[39] S. Ikeuchi, K. Saito, Y. Nakazawa, A. Sato, M. Mitsumi, K. Toriumi, and M. Sorai, Phys. Rev. B **66**, 115110 (2002).
[40] S. Ikeuchi, K. Saito, Y. Nakazawa, M. Mitsumi, K. Toriumi, and M. Sorai, J. Phys. Chem. **108**, 387 (2004).
[41] K. Saito, S. Ikeuchi, Y. Nakazawa, A. Sato, M. Mitsumi, T. Yamashita, K. Toriumi, and M. Sorai, J. Phys. Chem. B **109**, 2956 (2005).
[42] M. Kuwabara and K. Yonemitsu, J. Mater. Chem. **11**, 2163 (2001).
[43] S. Yamamoto, Phys. Rev. B **63**, 125124 (2001).
[44] S. Yamamoto, J. Phys. Soc. Jpn. **70**, 1198 (2001).
[45] S. Yamamoto, J. Phys. Chem. Solids **63**, 1489 (2002).
[46] S. Yamamoto and M. Ichioka, J. Phys. Soc. Jpn. **71**, 189 (2002).
[47] M. Kuwabara, K. Yonemitsu, and H. Ohta, in *EPR in the 21st Century*, edited by A. Kawamori, J. Yamaguchi, and H. Ohta (Elsevier Science, New York, 2002), p. 59.
[48] J. Ohara and S. Yamamoto, J. Phys. Soc. Jpn. **74**, 250 (2005).
[49] M. J. Hennessy, C. D. McElwee, and P. M. Richards, Phys. Rev. B **7**, 930 (1973).
[50] S. Kuroda, in *Organized Monolayers and Assemblies: Structure, Processes and Function, Studies in Interface Science*, Vol. 16, edited by D. Möbius and R. Miller (Elsevier, Amsterdam, 2002), Chap. 8.
[51] S. Kuroda, Adv. Colloid Interface Sci. **111**, 181 (2004).
[52] Y. Tomkiewicz and A. R. Taranko, Phys. Rev. B **18**, 733 (1978).
[53] Y. Tomkiewicz, Phys. Rev. B **19**, 4038 (1979).
[54] T. Takahashi, H. Doi, and H. Nagasawa, J. Phys. Soc. Jpn. **48**, 423 (1980).
[55] R. J. Elliott, Phys. Rev. **96**, 266 (1954).
[56] R. E. Deitz, F. R. Merritt, D. Dingle, R. Hone, B. G. Silvernagel, and P. M. Richards, Phys. Rev. Lett. **26**, 1186 (1971).
[57] P. M. Richards, Phys. Rev. B **10**, 805 (1974).
[58] A. Abragam and B. Bleaney, *Electron Paramagnetic Resonance of Transition Ions* (Clarendon Press, Oxford, 1970).
[59] A. Kawamori, R. Aoki, and M. Yamashita, J. Phys. C **18**, 5487 (1985).
[60] J. M. Assour, J. Chem. Phys. **43**, 2477 (1965).
[61] N. Kuroda, M. Ito, Y. Nishina, A. Kawamori, Y. Kodera, and T.

Matsukawa, Phys. Rev. B **48**, 4245 (1993).
[62] R. S. Alger, *Electron Paramagnetic Resonance: Techniques and Applications* (Interscience Publishers, New York, 1968).
[63] H. J. Pedersen, J. C. Scott, and K. Bechgaard, Phys. Rev. B **24**, 5014 (1981).
[64] M. Dumm, A. Loidl, B. Alavi, K. P. Starkey, L. K. Montgomery, and M. Dressel, Phys. Rev. B **62**, 6512 (2000).
[65] A. Abragam, *The Principles of Nuclear Magnetism* (Clarendon Press, Oxford, 1961) Chap. X.
[66] K. Marumoto, N. Takeuchi, T. Ozaki, and S. Kuroda, Synth. Met. **129**, 239 (2002).